Hodgkins Cell Classification Report
draft 1

Lihan Yao

Introduction

This paper analyzes high quality data arising from a Hodgkin's Lymphoma oncology study. The format consists of high-resolution microscopy images of tumor tissues under various states of reactivity to the same medical treatment. These tumor tissues and images were procured by the Ingo Mellinghoff Lab at Memorial Sloan Kettering Cancer Center as part of on-going oncology research. A natural machine learning task may be formulated as: given a multi-channel cell image where individual channels correspond to experimentally introduced biological markers, classify the cell between tumor/T-cell types, and if possible, the specific T-cell type.

A central difficulty to this task is the lack of a labeled dataset from which supervised learning traditionally proceeds. With help from MSK oncology researchers, we currently hold a labeled dataset of 80 samples. We maximize the usage of this human expertise by 1. selecting samples which optimally improved our baseline model and 2. applying data augmentation and model architectures specialized in utilizing unlabeled data.

Data

Due to the exotic nature of tumor cell image data, a central obstacle to training and evaluation has been access to a reliable labeled dataset. In addition, the acquisition of good data has traditionally been the most resource exhaustive component of data science projects. Special care has been taken to maximize the effort of human experts as mentioned in introduction.

Prior to the creation of a labeled dataset, we utilize HALO Image Analysis software for both cell detection (in the form of bounding boxes) and fuzzy labeling. By carefully viewing the tissue site through various biological markers, for one marker m, the researcher selected an appropriate threshold θ_m so that if a cell's average pixel intensity is above θ_m, it is 'labeled' positive for m. This is repeated for 31 biological markers. In this sense, a cell's class can be represented as a 31 dimensional 0/1 vector, and fuzzy, due to this threshold model's inherent variance. To support the on-going oncological research, we concern ourselves with four markers in particular. Moreover, we find cells with class vectors which are biologically impossible, but are nontheless informative. For these reasons, a cell may belong to oen of five potential classes. See appendix for an explanation of interpreting class labels.

Below is the pipeline for cell sample generation from raw images of the study.

Study contains 4 tumor tissues, each containing around 30 sites. For one site on the tissue, all cells are treated with various biological markers, digitally captured via a General Electric microscope

For one site, each of 32 greyscale marker images corresponds to a protein marker on the same spatial location of the tumor tissue, an example:

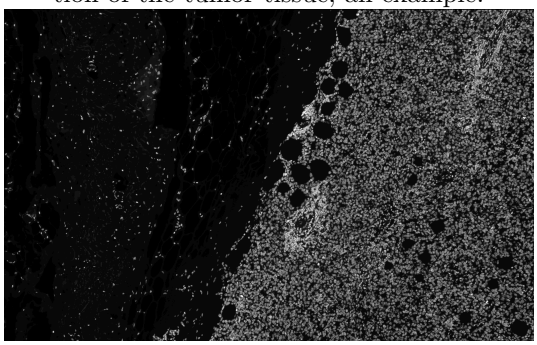

RGB Colored example using three greyscale images:

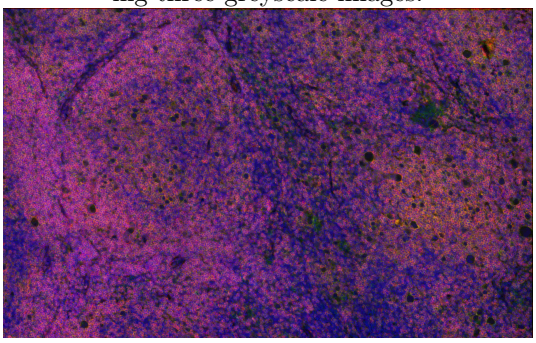

Using HALO Image Analysis, a CSV file containing cell bounding boxes as well as fuzzy labels for individual cells is used to create samples.

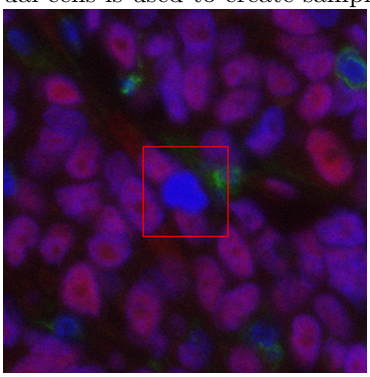

unlabeled samples

labeled samples

preprocessing (images rescaled to 50×50, $\mu \leftarrow 0, \sigma \leftarrow 1$)

data augmentation by rotation

A batch to be fed into the model then has the dimensions:

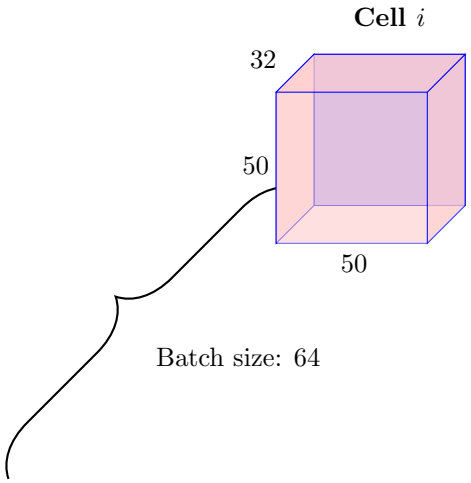

First the ladder network is trained on large labeled datasets whose labels are the fuzzy labels generated by the threshold model explained earlier. This is to distinguish a few hundred difficult samples to present to oncologists. We may then use these labeled samples to evaluate both models and begin a human-labeled dataset. The training set at this stage has 104,500 samples, with test set containing 41,000 and unlabeled set containing 260,800 samples, all after augmentation.

Model

Model selection is largely determined by three observations:

1. image samples have high number of channels and high resolution
2. human labeled dataset is a few hundred in size while unlabeled dataset is orders of magnitude larger.
3. augmenting cell image data by rotatation leads to new data which, to the human eye, is indistinguishable from original data

To take advantage of the last point, we quadruple labeled data by applying right angle rotations to individual samples. This practice was noted in Gao et al. (in the task of HEp-2 Cell Image Classification) to improve the model's rotational invariance. The second point hints at intricate nonlinear relationships which may arise from cell features. This suggests the complexity of a deep net is appropriate for the circumstance. In the area of image classification, ConvNets have been standard.

The first point, mainly that an ideal model should take advantage of the semi-supervised format, has put forth the Ladder Network as most fitting for our task, since it operates an unsupervised denoising task for representation learning, in addition to the original supervised task. To summarize why this works at a high level: the newly introduced denoising cost forces the encoder layers to find features efficient at generating latent representations close to the posterior distribution. A latent variable is 'pushed' to higher probabilities by our denoising function (learned by layers above).

Parameters of the encoder component (the feedforward component) is detailed below. Each convolutional layer introduces gaussian noise drawn from $\sim \mathcal{N}(\mu, 0.1)$ for the decoder to denoise. Each

layer of the encoder learns a representation of the noisy images. During model evaluation, holdout data is passed through these same layers without noise. The decoder reverses the convolutional layers of the encoder by deconvolution and mirrors the encoder configuration.

Table 1: Encoder component of the model

Layer Type	**Kernel**	**Output**	**Stride**	**Activation**	**Notes**
Conv	3X3	10	1	elu	Batchnorm prior to activation
Conv	3X3	20	1	elu	BN
Conv	3X3	40	1	elu	BN
Conv	3X3	80	1	elu	BN
MaxPool	2X2		2		
FullyConn		5			

Evaluation

At the time of writing, the ladder network has not been trained on human-labeled data. We find that our human-labeled dataset is only sufficiently large for model evaluation, even after data augmentation. Our model in the results below is trained on the dataset with fuzzy labeling.

The natural baseline to our ladder network is the threshold model whose parameters have been set by researchers via HALO. Though a labeled dataset is absent, we may evaluate the two models by FLOW: an experimental procedure which breaksdown the tumor tissue to classify cell-by-cell. If a model does not roughly match FLOW in distribution, we may conclude that misclassification is occuring.

Table 2: T-Cell types by percentage, computed experimentally and algorithmically

	CD3 %	**CD4 %**	**CD8 %**	**Total Cells Considered**
Threshold	91.7%	74.5%	13.6%	433327
Ladder Network	76%	67.1%	8.4%	49920
FLOW trial III	85%	74.6%	9.1%	436585
FLOW trial II	80.8%	71.1%	N/A	434822

In another evaluation approach, we select specific cell examples where the two models disagreed, and evaluate them individually by an oncologist.

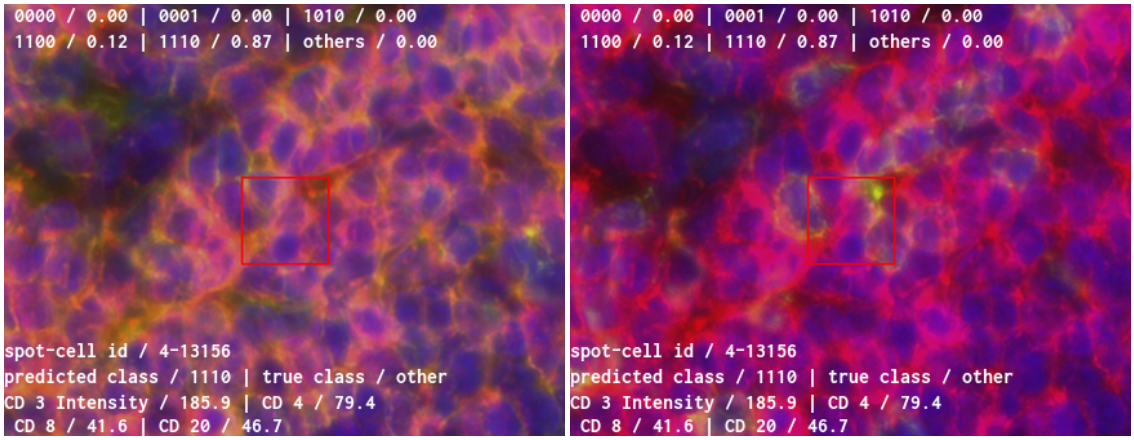

Figure 1: Three channel views of a captioned example where the models disagreed, with Ladder Network's class probabilities listed above

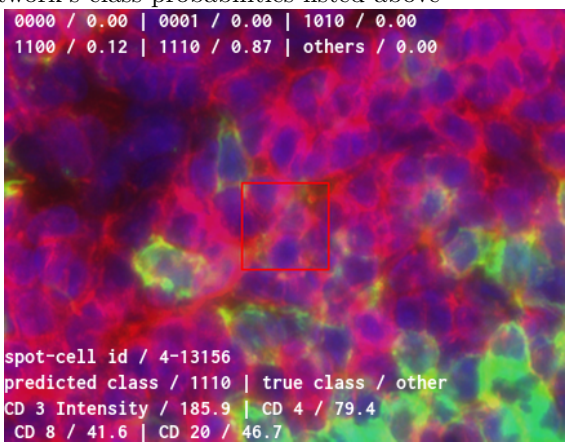

Discussion and Future Work

We showed initial progress towards a semi-supervised procedure using a dataset with limited label information. The approach employs data augmentation, utilization of vast amounts of unlabeled data, and sample priortization to optimize human labeling. Results of this deep learning model, as evaluated by FLOW and human cell-by-cell classifcation, show improvements over the threshold baseline.

Methods for decreasing the cost of domain-expertise labeling is much needed. As an auxiliary effort, we developed a cell-labeling program complete with keyboard shortcuts, channel view cycling, and image zoom. However, we find that more advanced features such as dynamic image manipulation, i.e. features commonly found in proprietary microscopy image analysis software such as HALO, to be highly helpful in data labeling.

Data augmentation methods beyond rotation should be tried. In the area of cell images, rotated synthetic data satisfies the important property of being indistinguishable from original data to the human eye. Future data augmentation should follow this principle to prevent model performance

degradation.

In comparison to a convolutional neural network, the ladder network has at least tripled the computation time for the same number of batches processed. A common operation throughout is batch normalization followed by nonlinear activation. An interesting experiment would be to substitute these two steps with a nonlinear activation function that can also implicitly normalize the activations. Very recent developments such as ELU (implemented in the current model alongside BN) and SELU claim to have this property with proper initializations.

Appendix

Model Parameter Choices

The first ladder network was worse computationally and performance-wise. The encoder component is detailed below:

Layer Type	**Kernel**	**Output**	**Stride**	**Activation**	**Notes**
Conv	3X3	20	1	elu	Batchnorm prior to activation
Conv	3X3	40	1	elu	BN
Conv	3X3	80	1	elu	BN
MaxPool	2X2		2		
fully-connected		5			

Given the complexity of cell images, it is better to have a deep network with thin layers. Prior to the development of a ladder network, a three layered vanilla ConvNet with batchnorm and dropout was developed (source code found in vanilla_convnet). With threshold labeled data, it attained 86% accuracy. However the large size disparity between human labeled and unlabeled datasets warranted the added complexity of the ladder network.

Cell segmentation, a common practice in microscopy image analysis, was also tried as a preprocessing step. The procedure zeros out low values in the cell tensor according to a special marker channel which contours the spatial geometry of cell bodies. The overall effect of this procedure is that most pixels outside of the cell membrane have been removed, so as to crop out the central cell. However, this was not used as a preprocessing step because the model suffered additional misclassification following this procedure.

Lastly, an important parameter is the gaussian noise introduced at every encoder layer. As noise increases, the encoder is forced to find more efficient or 'cleaner' representations, since the latent representation passed onto the decoder contains less signal. Experiments show that relative to the MNIST dataset, the tumor cell dataset is much more sensitive to noise. Noise drawn from gaussian distributions with larger variance than $\sim \mathcal{N}(\mu, 0.1)$ not only negatively affects the denoising task, but also supervised classification.

Interpreting Labels

Some combinations of CD3, CD4, CD8 and CD20 positivity are impossible, but at least one instance of every combination was found in the HALO CSV file. A combination of labels are encoded into binary as follows:

Table 3: Distribution of Threshold Labels

CD4, CD8, CD20	**Class Size**
101	241081
001	81264
100	34242
111	31275
011	22948
000	17676
110	3061
010	1780

$$\text{CD3 +, CD4 +, CD8 -, CD20 -} \xrightarrow{\text{binary}} \text{`1100}'$$

The first position always correspond to CD3 $+/-$, the second to CD4, and so on.

In confusion matrices, summing over a column such as '0000' yields the number of times our model predicted CD3 -, CD4 -, CD8 -, CD20 -. Summing over a row such as the first one, also corresponding to '000', yields the true number of CD3 -, CD4 -, CD8 -, CD20 - cells.

HALO Threshold Label Distribution

Distribution of threshold-generated labels is tabulated below.

Figure below consists of threshold labels organized by spots, where the x-axis correspond to decimal values of the binary strings.

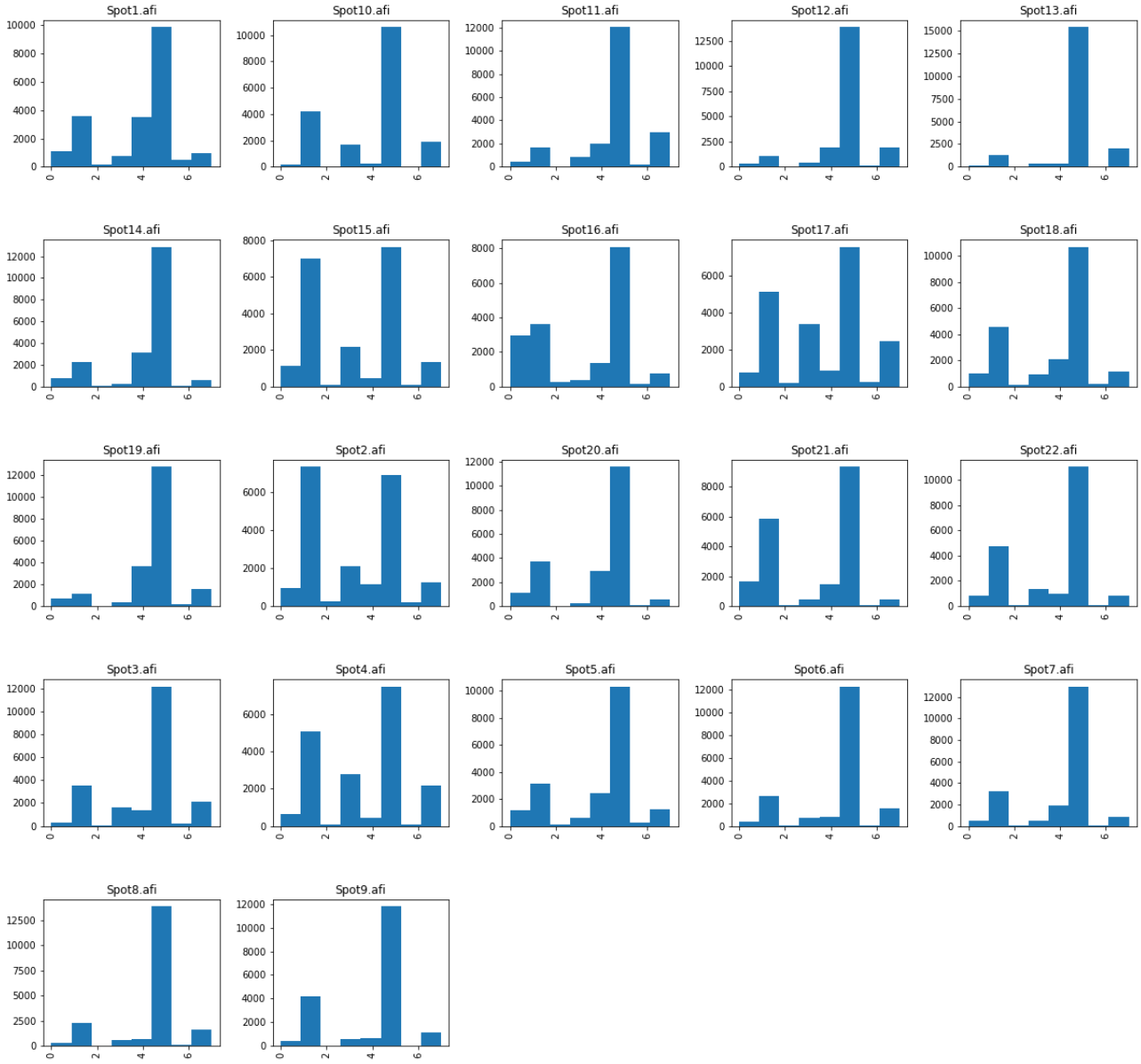
Spot1.afi
Spot10.afi
Spot11.afi
Spot12.afi
Spot13.afi
Spot14.afi
Spot15.afi
Spot16.afi
Spot17.afi
Spot18.afi
Spot19.afi
Spot2.afi
Spot20.afi
Spot21.afi
Spot22.afi
Spot3.afi
Spot4.afi
Spot5.afi
Spot6.afi
Spot7.afi
Spot8.afi
Spot9.afi